Journal of ELECTRONIC MATERIALS, Vol. 45, No. 6, 2016
DOI: 10.1007/s11664-016-4381-0

Temperature- and Hydrogen-Gas-Dependent Reversible Inversion of *n*-/*p*-Type Conductivity in CVD-Grown Multilayer Graphene (MLG) Film

D. DUTTA,[1,3] S.K. HAZRA,[2] J. DAS,[3] C.K. SARKAR,[1] and S. BASU[1,4]

1.—Department of ETCE, IC Design and Fabrication Centre, Jadavpur University, Kolkata, India. 2.—Department of Physics and Materials Science, Jaypee University of Information Technology (JUIT), Waknaghat, Himachal Pradesh, India. 3.—Department of Physics, Jadavpur University, Kolkata, India. 4.—e-mail: sukumarbasu@gmail.com

In atmospheric-pressure chemical vapor deposition-grown multilayer graphene films, a reversible change from *n*- to *p*-type conductivity has been observed in the temperature range of 25°C to 150°C upon exposure to hydrogen. This study was conducted with a simple Pd/graphene/Pd planar device. The inversion was observed at around 100°C, below which it showed stable *n*-type response to hydrogen. The hydrogen response was quite fast (1 s to 2 s) at 150°C. A plausible mechanism has been developed to explain such inversion. The selectivity and stability of the device in both *n*- and *p*-regions were investigated in the temperature range of 25°C to 150°C.

Key words: Multilayer graphene, CVD growth, planar device, *n*- to *p*-inversion, reversible response

INTRODUCTION

The ultimate criterion for a gas detector is to achieve single-molecule sensitivity with very fast response. This may become possible with the development of excellent sensor materials and reproducible device characteristics. Graphene is a novel material with very high surface-to-volume ratio, excellent thermal conductivity (~5000 W/m-K), and ultrahigh electrical mobility (~200,000 cm^2/V-s),[1] making this material an obvious choice for use in superfast gas sensor applications in the near future.[2–4] However, it is quite challenging to grow defect-free, ideal graphene matrix owing to certain limitations on the growth methods. Nevertheless, it is also possible to obtain gas sensors with very good response characteristics using defective graphene layers. In fact, defective layers enhance the gas adsorption kinetics, the first step towards efficient gas sensing. Atmospheric-pressure chemical vapor deposition (APCVD) is a convenient and cost-effective route for growth of graphene films.[5,6] Some reports are available on the hydrogen response of graphene.[2,7,8] Variation of the conductivity of the graphene matrix can be realized by doping.[9] Moreover, modulation of the type of electrical conductivity (*n*- or *p*-type) in undoped graphene may be possible through the contribution of the substrate and/or temperature. Romero et al. reported only *n*-type behavior for graphene deposited on SiO_2/Si substrate by easy electron transfer from SiO_2 to graphene owing to the low work function of SiO_2 compared with graphene.[10] Intercalation of few-layer graphene can also result in inversion in conductivity by inducing charge transfer from the substrate. Lao et al. reported the temperature-dependent far-infrared (FIR) response of both pristine and $FeCl_3$-intercalated graphene with reverse conductivity.[11] $FeCl_3$ behaves as an electron acceptor (i.e., creating holes), and electron transfer occurs from the substrate to graphene during FIR response. The influence of temperature on the conductivity was reported by Liu and coworkers when studying the nature of the temperature-dependent electrical resistance of few-layer graphene.[12] Similar to the electrical conductivity, the thermal conductivity of graphene is also

(Received October 7, 2015; accepted February 3, 2016; published online February 17, 2016)

temperature dependent. Xie et al. reported the temperature-dependent thermal conductivity of graphene nanoribbon (GNR) in the temperature range of −75°C to 100°C.[13] In GNR, increase of thermal conductivity and decrease of electrical resistance were found with increasing temperature.

In graphene, the type of electrical conductivity can also be modulated by variation of the temperature in an oxidizing or reducing atmosphere. A report is available on inversion of the conductivity type in graphene in the presence of an oxidizing atmosphere.[14] In this study, an attempt was made to correlate the inversion of the conductivity type of chemical vapor deposition (CVD)-grown multilayer graphene film on SiO_2/Si substrate with temperature in a reducing (hydrogen) atmosphere.

We employed the APCVD technique to deposit graphene thin films over SiO_2/Si substrates. The multilayer graphene film was characterized for composition and morphology using Raman spectroscopy, field-emission scanning electron microscopy (FESEM), and atomic force microscopy (AFM). A simple Pd/graphene/Pd planar device was fabricated by taking two lateral palladium (Pd) metal contacts over graphene. The temperature-dependent reversible inversion of conductivity (*n*- to *p*- and vice versa) of undoped graphene was studied in the range of 25°C to 150°C by exposing the planar device to different hydrogen concentrations (0.5%, 1.0%, and 2.0%) in air.

EXPERIMENTAL PROCEDURES

Graphene Deposition

Multilayer graphene was synthesized by the APCVD technique using equipment designed and fabricated in our laboratory.[15] A ∼300-nm-thick Cu film was deposited on the SiO_2/Si substrate by electron-beam evaporation. The Cu-coated SiO_2/Si substrates were then loaded into the CVD chamber. A flow of high-purity hydrogen (H_2) and nitrogen (N_2) mixture in the ratio of 25:500 (SCCM) was maintained in the chamber for 1 h at 1000°C to anneal the catalytic Cu metal film prior to graphene growth. Annealing of Cu was carried out to initiate grain growth of graphene on the substrate. The rates of heating (∼10°C/min) and cooling (∼5°C/min) were maintained using a programmable temperature controller. Graphene was grown at 1000°C by introducing methane (CH_4) gas as hydrocarbon source, along with the mixture of hydrogen and nitrogen. During growth for duration of 8 min, the H_2:CH_4:N_2 ratio was maintained at 25:10:300 (SCCM). After growth, the temperature of the substrates was reduced from 1000°C to 400°C at cooling rate of 5°C/min and then to room temperature by natural convection of heat after turning off the power to the furnace. Residual Cu on the substrates was removed by etching the samples using solution of 1 M ferric chloride ($FeCl_3$) in 1 M hydrochloric acid (HCl). Finally, the samples were repeatedly washed with deionized water in an ultrasonic cleaner and dried with hot dry air.

Characterization of Graphene

The graphene films were analyzed by Raman spectroscopy (LABRAM DILOR JY spectrometer, with 632.8-nm He-Ne laser source) to determine their nature. FESEM (JEOL JSM-6390LV) studies were carried out to reveal the surface morphology of the grown graphene films, and AFM (Nano-R2, Pacific Technology) was used to investigate the variation of the graphene surface with growth temperature.

Fabrication of Pd/Graphene/Pd Planar Device

Two lateral palladium (Pd) metal contacts with dimensions of 2 mm × 2 mm and thickness of 0.2 μm were deposited on the graphene surface using the e-beam evaporation technique after masking the device carefully with Al foil. Fine copper (Cu) wires and silver paste were subsequently used to achieve intimate electrical contacts.

Setup to Study Current–Voltage Characteristics

Temperature-dependent current–voltage (*I*–*V*) studies were carried out in a reducing atmosphere using a setup reported previously by us.[16] The experimental setup includes a stainless-steel tube for gas transmission. The gas flow rates were accurately controlled using mass flow controllers and mass flow meters (Digiflow, USA). The Pd/graphene/Pd planar device was placed inside a closed chamber (volume ∼95 cc) with 4 cm constant-temperature zone and gas inlet–outlet options. The planar device was connected directly to a Keithley picoammeter with voltage source (model 6487, M/S Keithley Instruments) to record the change in current during exposure to the hydrogen test gas at a certain applied voltage. The temperature was precisely controlled with ±1°C accuracy using a temperature controller (Aerials PID controller). High-purity gases [hydrogen (H_2, 99.998 vol.%), methane (CH_4, 99.99 vol.%), nitrogen (N_2, 99.99 vol.%), and air (oxygen ∼20 vol.% and nitrogen ∼80 vol.%)] were used for the present experiments. *I*–*V* measurements were performed using the Keithley picoammeter with built-in voltage source.

RESULTS AND DISCUSSION

Raman Spectroscopy

Presence of multilayer graphene was confirmed by the Raman spectra (Fig. 1). The prominent Raman signatures “D” (D-mode caused by disordered structure of graphene), “G” (G-band arising

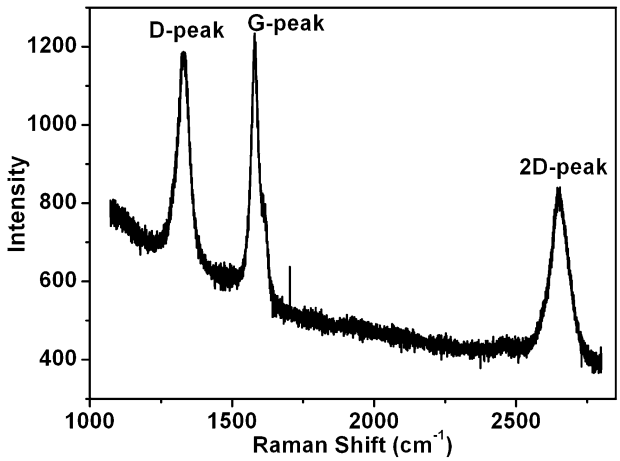

Fig. 1. Raman spectra of multilayer graphene grown by APCVD.

from stretching of C–C bonds in graphitic materials), and "2D" (2D-band corresponding to a second-order two-phonon process) imply the formation of multilayer defective graphene on SiO_2/Si substrates. The symmetric 2D band was positioned at 2650 cm^{-1}, and the D and G bands at 1328 cm^{-1} and 1580 cm^{-1}, respectively, close to reported values.[17] Any shift of the peaks from the ideal positions can be attributed to strain in the thin films induced by the substrate during the high-temperature CVD process because the thermal expansion coefficients of graphene and the substrate are different.[18,19]

The 2D band (2650 cm^{-1}) in the spectra is sharp and almost symmetrical. The ratio of the intensities of the 2D and G peaks for our samples is ~0.7, confirming the multilayer nature of the graphene. Only when this ratio is >2 can formation of monolayer graphene be confirmed. Also, the nature of the charge carriers or doping in graphene can be approximately estimated from the 2D peak position. According to Bruna et al., upshift of the 2D peak position implies hole doping, whereas electron doping causes downshift.[20] A 2D peak position at ~2690 cm^{-1} to 2700 cm^{-1} implies pristine nature of graphene.[14,21] Comparing the reported 2D peak position with that of our sample at 2650 cm^{-1} (Fig. 1), the possibility of electron doping of our grown graphene film may be envisaged because of the downshift of the 2D peak. This is further supported by the *n*-type conductivity of our as-grown samples.

The G band is due to the presence of sp^2-hybridized carbon bonds in the layers, and increase in the intensity of D band is due to an increasing number of graphene layers.[22] The D band indicates the presence of grain boundaries and defects in the graphene layer.[23] Furthermore, if the intensity ratio of the D to G band (I_D/I_G) is ~1, the presence of defects in the graphene matrix is highly likely. For our samples, the I_D/I_G value was ~0.8, indicating the presence of a large number of defects.

Surface Morphology

FESEM and AFM images of the surface of the APCVD-grown graphene are shown in Fig. 2. From the FESEM image presented in Fig. 2a, it appears that the graphene film has negligible undulations/cracks but exhibits occasional overgrowth. The AFM image shown in Fig. 2b indicates the topological appearance of our multilayer graphene samples. The scale on the *Y*-axis shows the variation in grain size. The color intensity signifies the density of the different grain sizes on the surface. The nonuniformity of the film is probably due to strain developed in the multilayer graphene film induced by the SiO_2/Si substrate during CVD growth at high temperature.[24] The morphology more or less corroborates the Raman spectroscopy studies. The topological disorder indicates the presence of defects in our multilayer graphene films. The I_D/I_G value (~0.8) obtained from the Raman spectra also confirms the topological observations by FESEM and AFM.

Response Characteristics in Air and Hydrogen Mixed with Air

We performed *I–V* characteristic experiments using Pd/graphene/Pd devices in the temperature range of 25°C to 150°C. The device was exposed to air or different concentrations of hydrogen (0.5%, 1.0%, and 2.0%) mixed with air in a closed chamber during *I–V* studies. *I–V* studies were carried out in both forward- and reverse-bias modes (Fig. 3) in the voltage range from −1 V to +1 V. At room temperature (25°C), the device showed *n*-type response in the presence of hydrogen gas mixed with air, with relatively higher response being observed at 50°C. However, the magnitude of the *n*-type response started to decrease at 75°C, and much weaker *n*-type response was found at 100°C. Interestingly, at 125°C, the response pattern reversed and the current value decreased upon exposure to hydrogen gas, thereby revealing a *p*-type characteristic, which was retained up to 150°C. Beyond 150°C, the response was very fast, and measurements could not be carried out accurately due to the limitations of our measurement system. During cooling, reversal of the response from *p*-type to *n*-type was observed at 100°C and below. Figure 3 clearly shows the transitions at different temperatures.

The hydrogen gas response was calculated as the ratio of the change in current ($I_g - I_a$) or ($I_a - I_g$) in the presence of hydrogen gas mixed with air (I_g) to the initial current in air (I_a) at constant bias voltage.[16] Repeated cycle transient responses were obtained for the various hydrogen concentrations (0.5%, 1.0%, and 2.0%) (Fig. 4). Experimental data were recorded only after dynamic equilibrium was attained at the corresponding voltage and steady temperature.

In multilayer graphene, hydrogen adsorption starts at relatively higher temperature, so we did

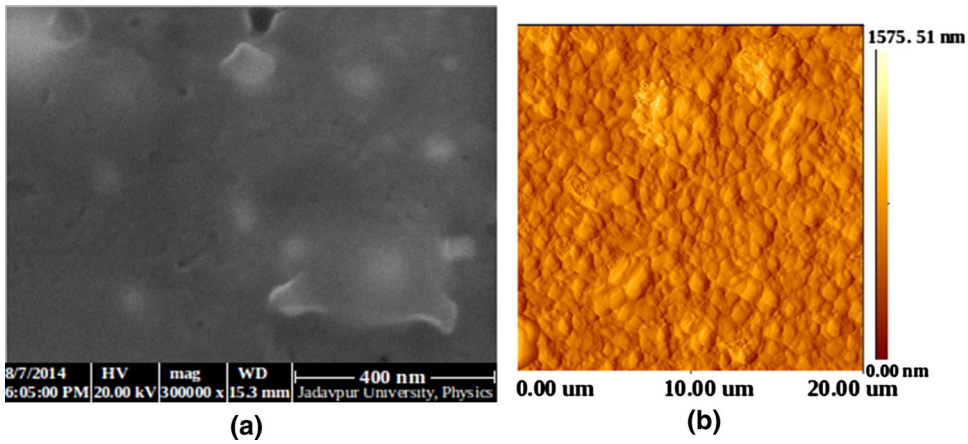

Fig. 2. (a) FESEM and (b) AFM images of multilayer graphene film grown by APCVD.

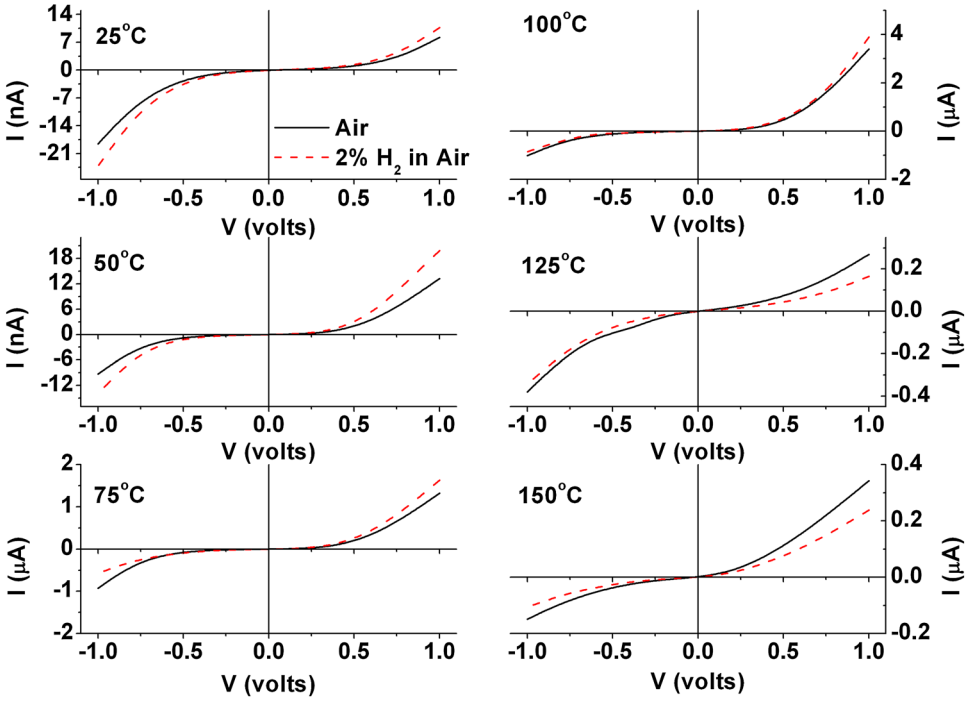

Fig. 3. Current–voltage (*I–V*) curves of Pd/graphene/Pd device in air and in 2% H_2 mixed with air in the temperature range of 25°C to 150°C.

not find much difference in the transient response with 0.5%, 1%, and 2% H_2 at 25°C and 50°C. At 75°C and 100°C, a distinct difference in current with increasing hydrogen concentration is visible in Fig. 4, perhaps due to reaching the hydrogen adsorption activation energy. After the transition in conductivity type above 100°C, the current was much lower, mostly due to carrier scattering and electron trapping during intercalation at higher temperature, and therefore the difference in the current response between the three different hydrogen concentrations could not be easily distinguished. This is apparent from the transient response behavior at 125°C and 150°C.

Two typical transient patterns, one at 50°C corresponding to *n*-type response and the other at 125°C where *p*-type response is prevalent, are presented in Fig. 5. Adequate saturation time of more than 1 min was given at both the top and bottom baseline levels.

Figure 6 presents the percentage response, the calculated response time for 90% change in signal upon exposure to hydrogen mixed with air, and the corresponding recovery time for reversal of the signal by 90% after the hydrogen supply was cut off.[16,25] A very fast (1 s to 2 s) response, high response magnitude, and fast recovery were found at 150°C (Fig. 6), where graphene showed *p*-type conductivity.

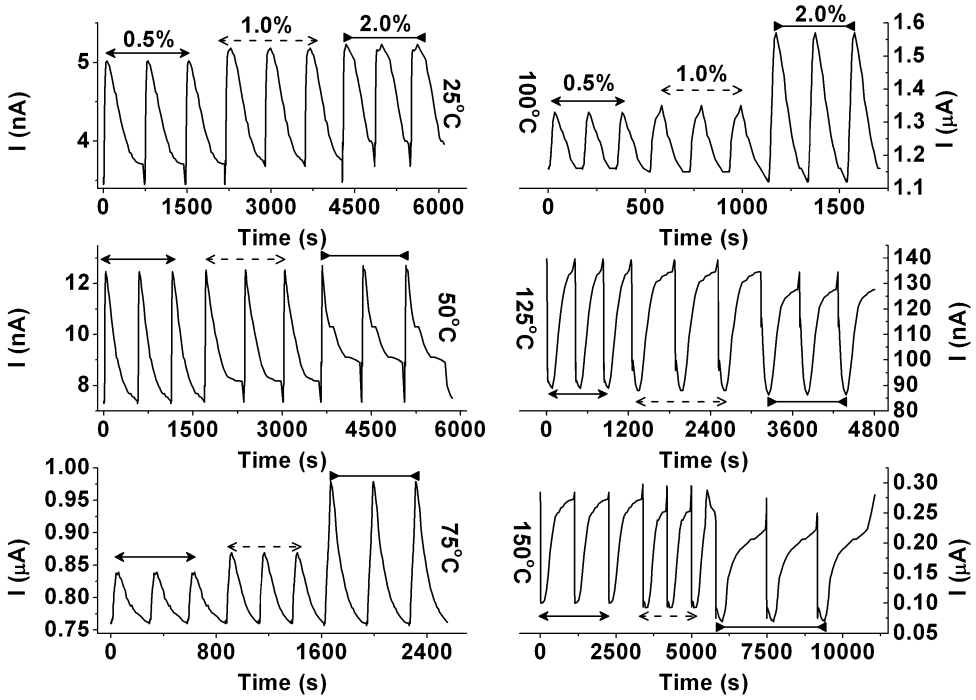

Fig. 4. Repeated cycle transient response patterns of Pd/graphene/Pd device in the temperature range of 25°C to 150°C upon exposure to different concentrations of hydrogen (0.5% to 2%) in air.

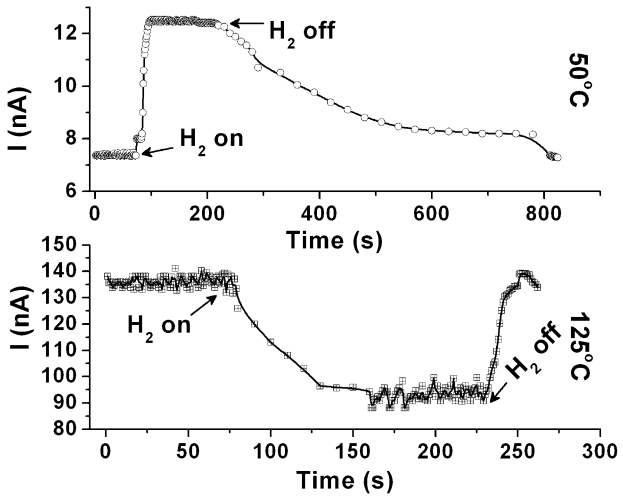

Fig. 5. Baseline response and saturation response at 50°C and 125°C for 1% H_2 in air.

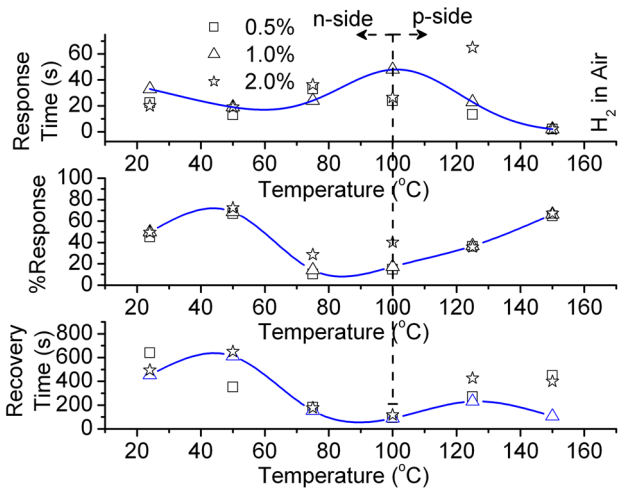

Fig. 6. Variation of response time, percentage response, and recovery time with temperature for 1% H_2 in air.

The Pd/graphene/Pd device showed 1% H_2 gas response to a maximum of ~72% at 50°C and ~68% at 150°C. Figure 6 demonstrates that the device can be conveniently used for hydrogen detection in air in the moderate-temperature region of around 150°C with quite high response magnitude, and appreciably fast response and recovery.

Figure 7 clearly demonstrates the reversible nature of the electrical conductivity in the temperature range of 25°C to 150°C.

The *n*-type response is clearly shown when the temperature is increased from room temperature. We find an increase in response up to 50°C, after which it starts decreasing. From 100°C, the response again starts increasing with *p*-type conductivity. This is an interesting observation that demonstrates the inversion in conductivity type in graphene with temperature in a reducing atmosphere. However, the percentage response remains almost the same during the heating cycle (room temperature to 150°C) as well as the cooling cycle (150°C to room temperature). This observation further confirms the accurate reversible nature of the conductivity transition in graphene. The

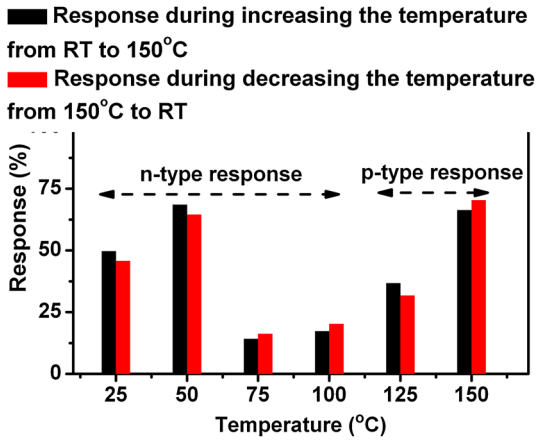

Fig. 7. 1% H_2 gas response during increasing and decreasing temperature with reversal of conductivity type (RT, room temperature).

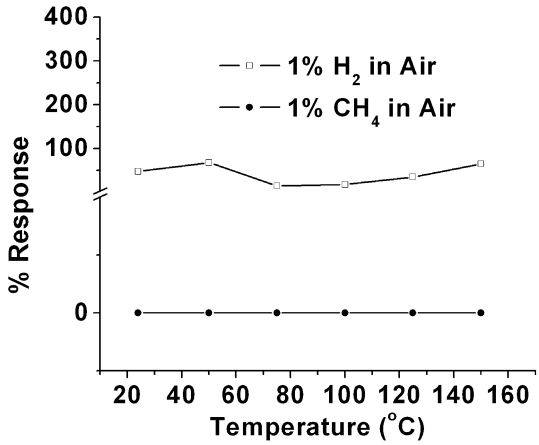

Fig. 8. Selective response of Pd/graphene/Pd planar device towards H_2 gas in presence of methane.

mechanism of conductivity inversion mentioned below in "Mechanism of Reversible *n*-/*p*-Inversion in Conductivity" section clarifies the reason as being due to electron exchange during adsorption and dissociation of hydrogen on graphene followed by electron trapping–detrapping phenomena.

Further study (Fig. 8) showed that hydrogen can be detected without any interference from methane, another reducing gas. Use of this kind of sensor is meaningful in coal mines, where both hydrogen and methane gases evolve and are present in the surrounding atmosphere.

The Pd/graphene/Pd device was exposed to 1% H_2 in air for 4 days at 50°C and also at 125°C in separate experiments, and the current was monitored while keeping the device at constant voltage (0.8 V). Figure 9 demonstrates that there was no deterioration in the current flowing through the device. Therefore, this simple device can be reliably used as a hydrogen leak detector.

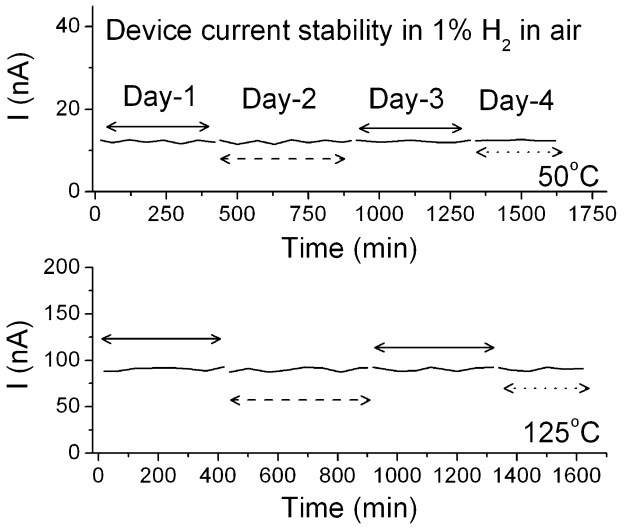

Fig. 9. Stable operation of the Pd/graphene/Pd planar device in 1% H_2 in air at 50°C and 125°C.

Mechanism of Reversible *n*-/*p*-Inversion in Conductivity

The conductivity inversion of the Pd/graphene/Pd planar device with temperature in the reducing atmosphere can be interpreted in the following simple and lucid manner:

In our study, graphene samples showed *n*-type conductivity at room temperature upon exposure to hydrogen (H_2) gas, as verified by Hall-effect experiments. We know that H_2 is a reducing gas and donates electrons to the graphene surface via dissociative adsorption. We deal with the Pd/graphene junction in the present study, and the presence of catalytic palladium (Pd) metal also likely enhances H_2 adsorption on the graphene surface and dissociation of hydrogen molecules (H_2) to hydrogen atoms (H). So, more electrons are donated to the graphene surface. Hence, we can say that exposure to a strong reducing gas such as hydrogen (H_2) increases the density of electrons, the majority carriers in graphene. This phenomenon is responsible for the *n*-type conductivity of graphene. Kim et al. also support this view in their report that graphene sheets, when exposed to H_2, are doped by electrons via dissociative adsorption of hydrogen molecules to hydrogen atoms. This phenomenon of electron doping in graphene upon exposure to hydrogen becomes more prominent as the number of graphene layers increases.[26] So, graphene samples with fewer layers, e.g., single-layer graphene (SLG) or bilayer graphene (BLG), seem to be weakly doped, whereas few-layer graphene (FLG) and multilayer graphene (MLG) seem to be strongly doped by electrons upon exposure to hydrogen gas.

However, at higher temperatures, this doping effect (due to the presence of H_2 gas) decreases as the gas desorption kinetics becomes quite strong with increase of temperature.[27] Again, for multilayer graphene, the desorption process should start

at relatively higher temperature compared with single- or bilayer graphene because the hydrogen adsorption is stronger for MLG as compared with SLG or BLG.[26] The desorption barrier for MLG increases with increase of the adsorbed gas molecules. So, both SLG and MLG samples initially show *n*-type conductivity upon exposure to hydrogen gas, but SLG loses its electron doping effect at relatively lower temperature (even room temperature) and exhibits *p*-type conductivity, while this loss occurs for MLG at significantly higher temperature, where the inversion occurs. This corroborates our experimental results of *n*- to *p*-type inversion for MLG samples in hydrogen mixed with air at higher temperatures. Further, on decreasing the temperature, the desorption rate decreases and adsorption dominates. As a result, *n*-type conductivity is recovered.

We would also like to present a more rigorous interpretation using the concept of bonds and bands and hydrogen intercalation in graphene. In graphene, three sp^2-hybridized orbitals are responsible for the σ-bonding in the *X*–*Y* plane, which leads to the formation of the hexagonal framework. The remaining *p*-orbital exists perpendicular to the *X*–*Y* plane, contributing one conduction electron per carbon (C) atom. Normally, graphene is a zero-bandgap material. However, the interface between the substrate and the first graphene monolayer results in a very small energy gap, and all semiconducting features develop due to this gap. In this study, a bandgap of 0.234 eV was determined for the grown graphene film by optical absorption spectroscopy. The semiconducting nature was also confirmed from the regular increase in device baseline current with increasing temperature in air ambient up to 100°C. The decrease in the baseline current beyond 100°C is probably due to the increase in carrier scattering at high temperatures (>100°C). Normally, if the carrier density of a material is very high, temperature-dependent metallic behavior is observed; i.e., the conductivity of the material decreases with increase in temperature due to the dominant effect of carrier scattering.[28,29] Graphene is a well-known high-carrier-density material, and normally electrons are the majority carriers. The electron concentration rises further due to Pd–hydrogen interaction. In the low-temperature regime (25°C to 100°C), the current is not greatly affected by carrier scattering. However, with increase in the temperature (above 100°C), the carrier scattering is enhanced. As a result, in air ambient and at elevated temperatures, a decrease in the baseline conductivity was observed.

The presented experimental results demonstrate a reversible transition (from *n*-type to *p*-type and vice versa) in hydrogen in the temperature range of 25°C to 150°C. The graphene device showed *n*-type conductivity up to 100°C, beyond which *p*-type conductivity was observed. Our graphene films are intrinsically electron doped, as indicated by the positions of the Raman signatures (Fig. 1), so the films have *n*-type conductivity at room temperature, as also determined by Hall-effect experiments. The inversion in the conductivity type on increasing the temperature can be explained by considering the effect of the SiO_2/Si substrate. Romero et al. reported that the *n*-type behavior of graphene film deposited on SiO_2/Si substrate[10] is due to the shift of the Fermi level above the Dirac point. Generally, this enhances easy electron transfer from SiO_2 to graphene.[10] Further, it is reported that *n*-type graphene samples are converted to *p*-type after exposure to strongly oxidizing gases such as O_2/NO_2.[30,31] This happens because adsorption of oxidant (O_2/NO_2) strongly depletes electrons from the sample, thus leading to a reduction in the majority carriers (electrons). So, a tendency to develop *p*-type conductivity is likely due to carrier trapping/annihilation. In a reducing ambient such as hydrogen in air, the opposite phenomenon can happen, i.e., the possibility of electron release/injection by trapping oxygen radicals from graphene surfaces/interfaces.[26] In the presence of palladium, such electron release/injection will be amplified because palladium is a good catalyst for hydrogen adsorption and subsequent dissociation. Therefore, for a Pd/(*n*-graphene)/Pd device, the dissociated hydrogen atoms may percolate down to the interface and release/inject electrons by trapping oxygen radicals. So, along with the substrate effect, a strong reducing gas such as hydrogen (H_2) enhances the electron concentration in the graphene matrix, hence a stronger *n*-type response is obtained with Pd/(*n*-graphene)/Pd junctions up to 100°C. However, beyond 100°C, the reversal in the type of hydrogen response (from *n*-type to *p*-type) is probably due to the enhanced Pd–hydrogen interaction and hydrogen intercalation in the graphene/SiO_2 substrate interface. Due to the stronger Pd–hydrogen interaction at elevated temperatures, the hydrogen concentration at the interface increases. At higher temperature, H atoms intercalate between the interface of the substrate and the first graphene monolayer, temporarily decoupling the graphene from the substrate (Fig. 10). This hinders the percolating hydrogen atoms from reaching the interface and preventing the process of release/injection of electrons (by trapping oxygen radicals). As a result, the reducing effect of hydrogen is diminished due to the temporary isolation, and the ambient again becomes oxidizing due to the presence of oxygen radicals at elevated temperatures. So, the released electrons are trapped by oxygen radicals, and *p*-type behavior is manifested. Using theoretical derivations with experimental support via scanning tunneling microscopy (STM), low-energy electron diffraction (LEED), and core-level photoelectron spectroscopy measurements, Riedl and coworkers confirmed the concept of temporary decoupling of a graphene monolayer after hydrogen intercalation at the Pd–graphene interface.[32] A

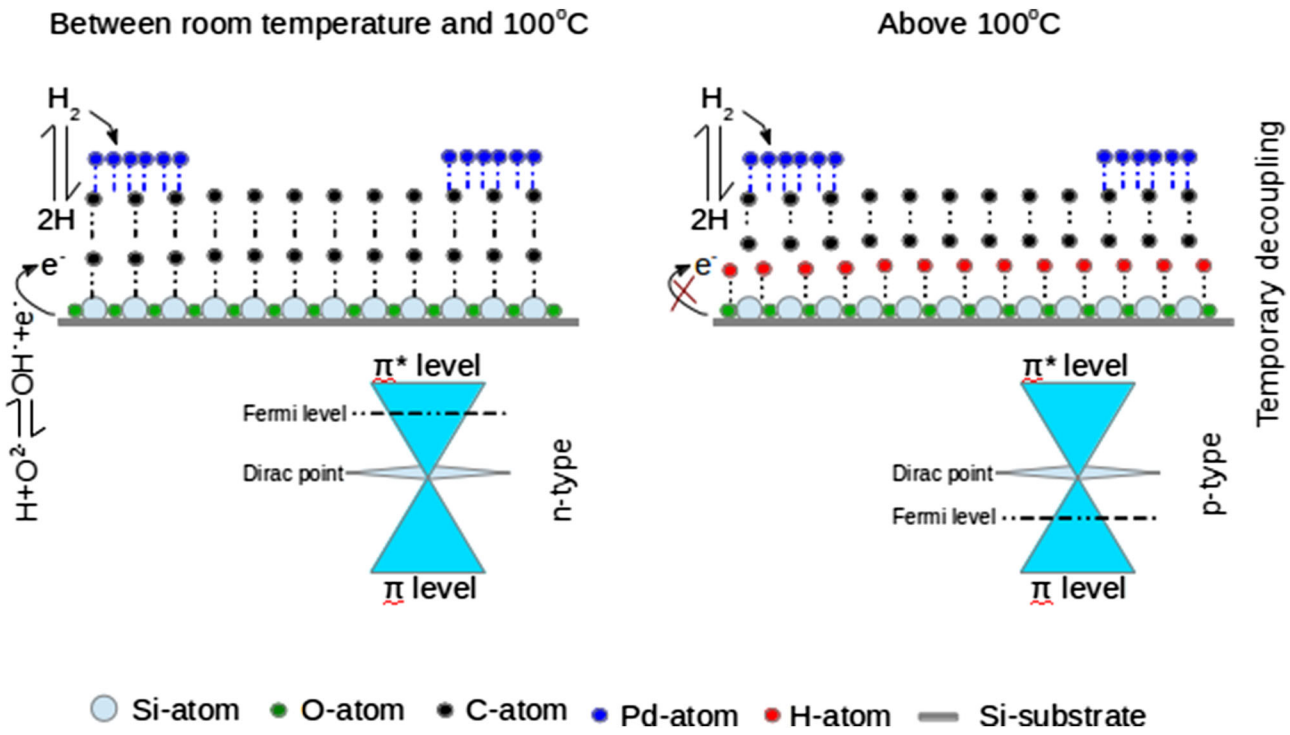

Fig. 10. Schematic of the hydrogen intercalation phenomenon.

similar concept of hydrogen intercalation of graphene has been reported by Watcharinyanon and coworkers.[33] They also used STM, LEED, and core-level photoelectron spectroscopy measurements to reveal that hydrogen atoms can go beneath the graphene primary layer and bond to Si atoms at the substrate interface. This is clarified by the schematic in Fig. 10.

The following equations are in good agreement with the above discussion:

$$H_2 \rightarrow 2H(ads) \quad \text{and} \quad H(ads) \rightarrow H^+ + e^- \quad (\text{hydrogen adsorption and dissociation}) \tag{1a}$$

$$O^- + (2H^+ + 2e^-) \rightarrow H_2O + e^- \quad (\text{electron freed and oxygen trapped}) \tag{1b}$$

$$O^- + e^- \rightarrow O^{2-} \quad (\text{electron trapped by oxygen radical during intercalation}) \tag{1c}$$

As stated above, reports on conductivity inversion in graphene in oxidizing environments are available in literature.[30,31] In the present investigation, the temperature-dependent conductivity inversion of multilayer graphene in a reducing atmosphere is based on experimental observations and theoretical understanding.

CONCLUSIONS

In APCVD-grown multilayer graphene, a reversible conductivity transition from *n*- to *p*-type was observed at 100°C in air atmosphere containing low concentration of hydrogen, as verified by fabricating a simple Pd/graphene/Pd planar device and operating it in 0.5%, 1%, and 2% hydrogen mixed with air in the temperature range of 25°C to 150°C. The *p*-type response for hydrogen beyond 100°C was relatively faster compared with the *n*-type response. A detailed mechanism has been presented to explain the temperature-dependent inversion of the conductivity in the presence of hydrogen. The reliability of this simple graphene-based device in terms of its reproducible nature and selective hydrogen response along with stable operation up to 150°C may be encouraging to develop hydrogen leak detectors to operate far below the explosion limit of hydrogen (~4% in air).

ACKNOWLEDGEMENTS

This work was taken up with a sponsored research programme financed by CSIR, Govt. of India and UGC, Govt. of India. D.D. gratefully acknowledges a junior research fellowship from CSIR. S.K.H. is thankful to Prof. C.K Sarkar, Coordinator, IC Design & Fabrication Center, Dept. of ETCE, Jadavpur University, India for providing a collaborative research opportunity. The authors are thankful to Prof. E. Bontempi (INSTM and Dipartimento di Ingegneria Meccanica ed Industriale), Brescia University, Italy and Prof. S.K. Sinha, Dept.

of Physics and Dept. of Electrical Engg., University of New Haven, USA for providing Raman and AFM results, respectively, for our graphene samples.

REFERENCES

1. S. Basu and P. Bhattacharyya, *Sens. Actuators B* 173, 1 (2012).
2. W. Wu, Z. Liu, L.A. Jauregui, Q. Yu, R. Pillai, H. Caoc, J. Bao, Y.P. Chen, and S. Pei, *Sens. Actuators B* 150, 296 (2010).
3. F. Yavari, E. Castillo, H. Gullapalli, P.M. Ajayan, and N. Koratka, *Appl. Phys. Lett.* 100, 203120 (2012).
4. C.W. Chen, S.C. Hung, M.D. Yang, C.W. Yeh, C.H. Wu, G.C. Chi, F. Ren, and S.J. Pearton, *Appl. Phys. Lett.* 99, 243502 (2011).
5. A. Ismach, C. Druzgalski, S. Penwell, A. Schwartzberg, M. Zheng, A. Javey, J. Bokor, and Y. Zhang, *Nano Lett.* 10, 1542 (2010).
6. C.Y. Su, A.Y. Lu, C.Y. Wu, Y.T. Li, K.K. Liu, W. Zhang, S.Y. Lin, Z.Y. Juang, Y.L. Zhong, F.R. Chen, and L.J. Li, *Nano Lett.* 11, 3612 (2011).
7. R. Kumar, D. Varandani, B.R. Mehta, V.N. Singh, Z. Wen, X. Feng, and K. Mullen, *Nanotechnology* 22, 275719 (2011).
8. M.G. Chung, D. Kim, D.K. Seo, T. Kim, H.U. Im, H.M. Lee, J. Yoo, S. Hong, T.J. Kang, and Y.H. Kim, *Sens. Actuators B* 169, 387 (2012).
9. X. Meng, S. Tongay, J. Kang, Z. Chen, F. Wu, S.S. Li, J.B. Xia, J. Li, and J. Wu, *Carbon* 57, 507 (2013).
10. H.E. Romero, N. Shen, P. Joshi, H.R. Gutierrez, S.A. Tadigadapa, J.O. Sofo, and P.C. Eklund, *ACS Nano* 2, 2037 (2008).
11. Y.F. Lao, A.G.U. Perera, K. Shepperd, F. Wang, E.H. Conrad, and M.D. Williams, *Appl. Phys. Lett.* 102, 231906 (2013).
12. Y. Liu, Z. Liu, W.S. Lew, and Q.J. Wang, *Nanoscale Res. Lett.* (2013). doi:10.1186/1556-276X-8-335.
13. H. Xie, L. Chen, W. Yu, and B. Wang, *Appl. Phys. Lett.* 102, 111911 (2013).
14. R. Jaaniso, T. Kahro, J. Kozlova, J. Aarik, L. Aarik, H. Alles, A. Floren, A. Gerst, A. Kasilov, A. Niilisk, and V. Sammelselg, *Sens. Actuators B* 190, 1006 (2014).
15. D. Dutta, A. Hazra, J. Das, S.K. Hazra, V.N. Lakshmi, S.K. Sinha, A. Gianonchelli, C.K. Sarkar, and S. Basu, *J. Nanomater. Mol. Nanotechnol.* (2013). doi:10.4172/2324-8777.
16. D. Dutta, S.K. Hazra, J. Das, C.K. Sarkar, and S. Basu, *Sens. Actuators B* 212, 84 (2015).
17. Y.G. Sun, H.H. Wang, and M.G. Xia, *J. Phys. Chem. C* 112, 1250 (2008).
18. A.C. Ferrari, J.C. Meyer, V. Scardaci, C. Casiraghi, M. Lazzeri, F. Mauri, S. Piscanec, D. Jiang, K.S. Novoselov, S. Roth, and A.K. Geim, *Phys. Rev. Lett.* 97, 187401 (2006).
19. C.C. Chen, W.Z. Bao, J. Theiss, C. Dames, C.N. Lau, and S.B. Cronin, *Nano Lett.* 9, 4172 (2009).
20. M. Bruna, A.K. Ott, M. Ija, D. Yoon, U. Sassi, and A.C. Ferrari, *ACS Nano* 8, 7432 (2014).
21. P.N. Incze, G. Magda, K. Kamaras, and L.P. Bir, *Nano Res.* (2010). doi:10.1007/s12274-010-1015-3.
22. Z. Luo, T. Yu, K.J. Kim, Z. Ni, Y. You, S. Lim, Z. Shen, S. Wang, and J. Lin, *ACS Nano* 3, 1781 (2009).
23. T. Cui, R. Lv, Z.H. Huang, H. Zhu, Y. Jia, S. Chen, K. Wang, D. Wu, and F. Kang, *Nanoscale Res. Lett.* (2012). doi:10.1186/1556-276X-7-453.
24. P.N. Incze, G. Magda, K. Kamarás, and L.P. Biró, *Nano Res.* (2010). doi:10.1007/s12274-010-1015-3.
25. D. Gupta, D. Dutta, M. Kumar, P.B. Barman, C.K. Sarkar, S. Basu, and S.K. Hazra, *Sens. Actuators B* 196, 215 (2014).
26. B.H. Kim, S.J. Hong, S.J. Baek, H.Y. Jeong, N. Park, M. Lee, S.W. Lee, M. Park, S.W. Chu, H.S. Shin, J. Lim, J.C. Lee, Y. Jun, and Y.W. Park, *Sci. Rep.* (2012). doi:10.1038/srep00690.
27. A. Hazra, S. Das, J. Kanungo, C.K. Sarkar, and S. Basu, *Sens. Actuators B* 183, 87 (2013).
28. K.I. Bolotin, K.J. Sikes, J. Hone, H.L. Stormer, and P. Kim, *Phys. Rev. Lett.* 101, 096802 (2008).
29. Y.W. Tan, Y. Zhang, K. Bolotin, Y. Zhao, S. Adam, E.H. Hwang, S. Das Sarma, H.L. Stormer, and P. Kim, *Phys. Rev. Lett* 99, 246803 (2007).
30. R. Pearce, T. Iakimov, M. Andersson, L. Hultman, A. Lloyd Spetz, and R. Yakimova, *Sens. Actuators B* 155, 451 (2011).
31. H.Y. Jeong, D.S. Lee, H.K. Choi, D.H. Lee, J.E. Kim, J.Y. Lee, W.J. Lee, S.O. Kim, and S.Y. Choi, *Appl. Phys. Lett.* 96, 213105 (2010).
32. C. Riedl, C. Coletti, and U. Starke, *J. Phys. D Appl. Phys.* 43, 374009 (2010).
33. S. Watcharinyanon, C. Virojanadara, J.R. Osiecki, A.A. Zakharov, R. Yakimova, R.I.G. Uhrberg, and L.I. Johansson, *Surf. Sci.* 605, 1662 (2011).